From proteomics to discovery of first-in-class ST2 inhibitors active in vivo

Abdulraouf M. Ramadan[1], Etienne Daguindau[1], Jason C. Rech[2], Krishnapriya Chinnaswamy[3], Jilu Zhang[1], Greg L. Hura[3,4], Brad Griesenauer[1], Zachary Bolten[1], Aaron Robida[5], Martha Larsen[5], Jeanne A. Stuckey[5,6], Chao-Yie Yang[2*] & Sophie Paczesny[1*]

[1]Department of Pediatrics and Immunology, Indiana University School of Medicine, Indianapolis, IN 46202, USA.

[2]Department of Internal Medicine, Hematology and Oncology Division, University of Michigan, Ann Arbor, MI 48109, USA.

[3]Lawrence Berkeley National Laboratory, Berkeley, CA 94720, USA.

[4]Department of Chemistry and Biochemistry, University of California, Santa Cruz, Santa Cruz, CA 95064, USA.

[5]Life Science Institute, University of Michigan, MI 48109, USA.

[6]Department of Biological Chemistry, University of Michigan, Ann Arbor, MI 48109, USA.

Supplemental Material

Methods

Chemical Reagents in High-Throughput Screening. Compounds used in high-throughput screening (HTS) were provided by the Indiana University School of Medicine, Chemical Core Facility. Chemical reagents used in confirmatory screening (45 compounds) and hits enrichment (118 compounds) were purchased from commercial sources. The vendors included ChemBridge, ChemDiv, Analyticon Discovery and Chem-X Infinity. iST2-1(ChemDiv), iST2-2 (ChemBridge) and iST2-3(ChemDiv) used in the in vivo disease model studies were resynthesized by the vendors at 1 gram each. The purities of these compounds were ≥90%.

Chemical Syntheses and Characterization of iST2-1 and its Analogs. All reagents were purchased from Sigma-Aldrich or Combi-Blocks and used as is. All purification was accomplished using a Teledyne ISCO CombiFlash® system employing RediSep® Rf Media silica gel columns.

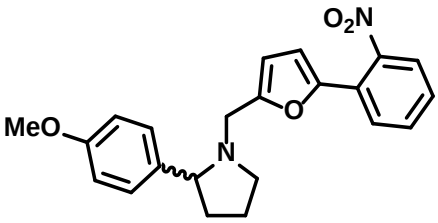

iST2-1

(R/S)-2-(4-methoxyphenyl)-1-((5-(2-nitrophenyl)furan-2-yl)methyl)pyrrolidine, iST2-1: To a solution of (R/S)-2-(4-methoxyphenyl)pyrrolidine (100 mg, 0.564 mmol) and 5-(2-nitrophenyl)furan-2-carbaldehyde (119 mg, 0.564 mmol) in dichloromethane was added triacetoxyborohydride (359 mg, 1.692 mmol), and the resulting reaction mixture was stirred overnight at room temperature. Saturated aqueous sodium bicarbonate solution was added (10 mL), and the resulting reaction mixture was extracted with dichloromethane (3 × 10 mL). The organic layers were combined, dried with Na_2SO_4, filtered, concentrated and purified by flash column chromatography (0-100% EtOAc in hexanes) to provide the desired product (163 mg, 77%). MS calcd for $C_{22}H_{22}N_2O_4$ found 379.21 (M+H); ^{1}H NMR (400 MHz, DMSO-d_6) δ 7.87 (dd, *J* = 8.1, 1.2 Hz, 1H), 7.80 (dd, *J* = 7.8, 1.4 Hz, 1H), 7.77 – 7.67 (m, 1H), 7.55 (ddd, *J* = 8.1, 7.4, 1.4 Hz, 1H), 7.34 – 7.25 (m, 2H), 6.94 – 6.86 (m, 2H), 6.84 (d, *J* = 3.4 Hz, 1H), 6.35 (d, *J* = 3.4 Hz, 1H), 3.75 (s, 3H), 3.63 (d, *J* = 14.7 Hz, 1H), 3.36 (dd, *J* = 8.7, 7.5 Hz, 1H), 3.24 (d, *J* = 14.6 Hz, 1H), 3.10 (ddd, *J* = 10.9, 8.1, 2.8 Hz, 1H), 2.38 (q, *J* = 8.8 Hz, 1H), 2.09 (dddd, *J* = 12.4, 9.3, 7.5, 5.0 Hz, 1H), 1.90 – 1.65 (m, 2H), 1.53 (dddd, *J* = 12.3, 10.5, 8.8, 6.3 Hz, 1H).

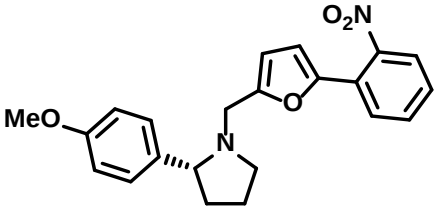

(R)-iST2-1

(R)-2-(4-methoxyphenyl)-1-((5-(2-nitrophenyl)furan-2-yl)methyl)pyrrolidine, (R)-iST2-1: See procedure for (R/S)-2-(4-methoxyphenyl)-1-((5-(2-nitrophenyl)furan-2-

yl)methyl)pyrrolidine. MS calcd for $C_{22}H_{22}N_2O_4$ found 379.24 (M+H); $[\alpha]_D^{25}$ = +106.2; ^{1}H NMR (400 MHz, DMSO-d_6) δ 7.87 (dd, *J* = 8.1, 1.1 Hz, 1H), 7.83 – 7.78 (m, 1H), 7.72 (ddd, *J* = 7.9, 7.4, 1.2 Hz, 1H), 7.56 (ddd, *J* = 8.1, 7.4, 1.4 Hz, 1H), 7.34 – 7.27 (m, 2H), 6.93 – 6.87 (m, 2H), 6.84 (d, *J* = 3.4 Hz, 1H), 6.35 (d, *J* = 3.3 Hz, 1H), 3.75 (s, 3H), 3.63 (d, *J* = 14.7 Hz, 1H), 3.43 – 3.34 (m, 1H), 3.24 (d, *J* = 14.6 Hz, 1H), 3.10 (td, *J* = 8.4, 2.8 Hz, 1H), 2.38 (q, *J* = 8.7 Hz, 1H), 2.16 – 2.03 (m, 1H), 1.90 – 1.66 (m, 2H), 1.62 – 1.45 (m, 1H).

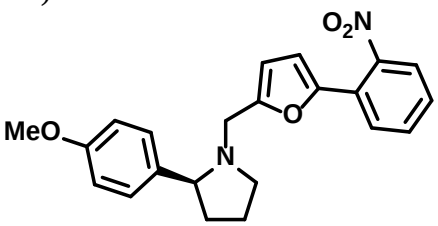

(S)-iST2-1

(S)-2-(4-methoxyphenyl)-1-((5-(2-nitrophenyl)furan-2-yl)methyl)pyrrolidine, (S)-iST2-1: See procedure for (R/S)-2-(4-methoxyphenyl)-1-((5-(2-nitrophenyl)furan-2-yl)methyl)pyrrolidine. MS calcd for $C_{22}H_{22}N_2O_4$ found 379.26 (M+H)**;** $[\alpha]_D^{25}$ = -104.8: ^{1}H NMR (400 MHz, DMSO-d_6) δ 7.87 (dd, *J* = 8.1, 1.2 Hz, 1H), 7.80 (dd, *J* = 7.9, 1.4 Hz, 1H), 7.72 (td, *J* = 7.6, 1.3 Hz, 1H), 7.56 (ddd, *J* = 8.1, 7.4, 1.4 Hz, 1H), 7.34 – 7.27 (m, 2H), 6.96 – 6.87 (m, 2H), 6.84 (d, *J* = 3.4 Hz, 1H), 6.35 (d, *J* = 3.4 Hz, 1H), 3.75 (s, 3H), 3.63 (d, *J* = 14.7 Hz, 1H), 3.37 (dd, *J* = 8.7, 7.5 Hz, 1H), 3.24 (d, *J* = 14.7 Hz, 1H), 3.14 – 3.06 (m, 1H), 2.38 (q, *J* = 8.7 Hz, 1H), 2.08 (ddt, *J* = 12.4, 8.3, 4.5 Hz, 1H), 1.91 – 1.66 (m, 2H), 1.60 – 1.47 (m, 1H).

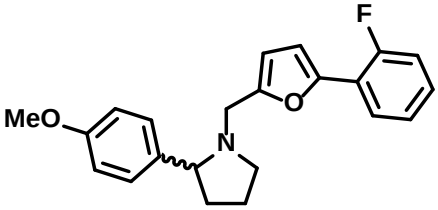

iST2-1F

(R/S)1-((5-(2-fluorophenyl)furan-2-yl)methyl)-2-(4-methoxyphenyl)pyrrolidine, iST2-1F: See procedure for (R/S)-2-(4-methoxyphenyl)-1-((5-(2-nitrophenyl)furan-2-yl)methyl)pyrrolidine. MS calcd for $C_{22}H_{22}FNO_2$ found 352.21 (M+H); ^{1}H NMR (400 MHz, DMSO-d_6) δ 7.76 – 7.68 (m, 1H), 7.38 – 7.27 (m, 5H), 6.96 – 6.86 (m, 2H), 6.76 (t, *J* = 3.5 Hz, 1H), 6.36 (d, *J* = 3.3 Hz, 1H), 3.75 (s, 3H), 3.70 (d, *J* = 14.6 Hz, 1H), 3.40 – 3.29 (m, 2H), 3.20 – 3.12 (m, 1H), 2.43 (q, *J* = 8.8 Hz, 1H), 2.16 – 2.03 (m, 1H), 1.89 – 1.66 (m, 2H), 1.64 – 1.50 (m, 1H).

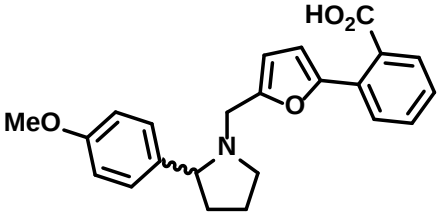

iST2-2

(R/S)-2-(5-((2-(4-methoxyphenyl)pyrrolidin-1-yl)methyl)furan-2-yl)benzoic acid, iST2-2: See procedure for (R/S)-2-(4-methoxyphenyl)-1-((5-(2-nitrophenyl)furan-2-yl)methyl)pyrrolidine. ^{1}H NMR (400 MHz, DMSO-d_6) δ 10.26 (s, 1H), 7.76 – 7.39 (m, 6H), 7.03 (d, *J* = 8.4 Hz, 2H), 6.76 (s, 2H), 4.46 (s, 1H), 4.23 (s, 2H), 3.78 (s, 3H), 3.65 (s, 1H), 2.42 (s, 1H), 2.12 (s, 3H).

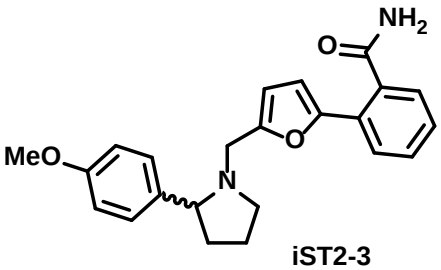

iST2-3

2-(5-((2-(4-methoxyphenyl)pyrrolidin-1-yl)methyl)furan-2-yl)benzamide, iST2-3: To a solution of (R/S)-2-(5-((2-(4-methoxyphenyl)pyrrolidin-1-yl)methyl)furan-2-yl)benzonitrile (100 mg, 0.289 mmol) in ethanol (5 mL) and water (1 mL) was added hydrido(dimethylphosphinous acid-kP)[hydrogen bis(dimethylphosphinito-kP)]platinum(II) (6 mg, 0.014 mmol) and the reaction mixture was heated to 80 °C for 16 hours. The reaction mixture was cooled to rt, filtered through a pad of celite and concentrated to provide the desired product in 94% yield (102 mg). ^{1}H NMR (400 MHz, DMSO-d_6) δ 7.82 (s, 1H), 7.64 (dt, *J* = 7.9, 0.9 Hz, 1H), 7.51 – 7.40 (m, 2H), 7.36 – 7.28 (m, 4H), 6.96 – 6.89 (m, 2H), 6.69 (d, *J* = 3.3 Hz, 1H), 6.27 (d, *J* = 3.3 Hz, 1H), 3.76 (s, 3H), 3.67 (d, *J* = 14.6 Hz, 1H), 3.37 (t, *J* = 8.2 Hz, 1H), 3.26 (d, *J* = 14.5 Hz, 1H), 3.20 – 3.13 (m, 1H), 2.43 (q, *J* = 8.8 Hz, 1H), 2.18 – 2.01 (m, 1H), 1.91 – 1.67 (m, 2H), 1.63 – 1.49 (m, 1H).

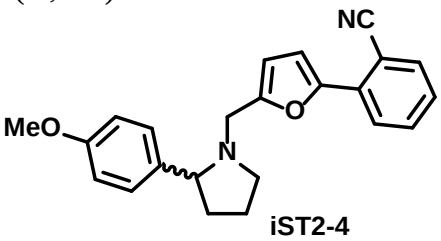

iST2-4

(R/S)-2-(5-((2-(4-methoxyphenyl)pyrrolidin-1-yl)methyl)furan-2-yl)benzonitrile, iST2-4: See procedure for (R/S)-2-(4-methoxyphenyl)-1-((5-(2-nitrophenyl)furan-2-yl)methyl)pyrrolidine. ^{1}H NMR (400 MHz, DMSO-d_6) δ 7.89 (ddd, *J* = 7.8, 1.4, 0.5 Hz, 1H), 7.84 (ddd, *J* = 8.1, 1.3, 0.6 Hz, 1H), 7.81 – 7.75 (m, 1H), 7.47 (td, *J* = 7.5, 1.3 Hz, 1H), 7.37 – 7.29 (m, 2H), 7.16 (d, *J* = 3.4 Hz, 1H), 6.93 – 6.83 (m, 2H), 6.43 (d, *J* = 3.4 Hz, 1H), 3.74 (s, 3H), 3.71 (d, *J* = 15.4 Hz, 1H), 3.39 (dd, *J* = 8.9, 7.6 Hz, 1H), 3.36 – 3.30 (m, 1H), 3.24 – 3.14 (m, 1H), 2.44 (q, *J* = 8.8 Hz, 1H), 2.10 (dddd, *J* = 12.4, 9.3, 7.4, 5.0 Hz, 1H), 1.91 – 1.66 (m, 2H), 1.63 – 1.47 (m, 1H).

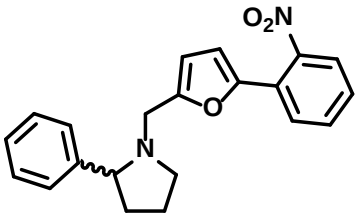

iST2-5

(R/S)-1-((5-(2-nitrophenyl)furan-2-yl)methyl)-2-phenylpyrrolidine, iST2-5: See procedure for (R/S)-2-(4-methoxyphenyl)-1-((5-(2-nitrophenyl)furan-2-yl)methyl)pyrrolidine. ^{1}H NMR (400 MHz, DMSO-d_6) δ 7.87 (dd, *J* = 8.1, 1.2 Hz, 1H), 7.80 (dd, *J* = 7.8, 1.4 Hz, 1H), 7.72 (td, *J* = 7.6, 1.2 Hz, 1H), 7.56 (ddd, *J* = 8.0, 7.4, 1.4 Hz, 1H), 7.43 – 7.37 (m, 2H), 7.37 – 7.32 (m, 2H), 7.28 – 7.22 (m, 1H), 6.85 (d, *J* = 3.3 Hz, 1H), 6.36 (d, *J* = 3.4 Hz, 1H), 3.65 (d, *J* = 14.6 Hz, 1H), 3.44 (t, *J* = 8.1 Hz, 1H), 3.26

(d, *J* = 14.6 Hz, 1H), 3.11 (ddd, *J* = 8.9, 7.8, 2.9 Hz, 1H), 2.41 (q, *J* = 8.7 Hz, 1H), 2.21 – 2.08 (m, 1H), 1.89 – 1.68 (m, 2H), 1.55 (dddd, *J* = 12.3, 10.4, 8.7, 6.2 Hz, 1H).

Thermofluor Assay. Two constructs of ST2 (residues 19-323 and 19-206) were purified as previously described (1). To determine the optimal concentrations of ST2 and dye concentrations for binding detection, three concentrations of ST2 (residue 19-323, at 0.1 mg/mL, 0.2 mg/mL and 0.4 mg/mL) in 10 mM HEPES 7.2, 150 mM NaCl were mixed with three dyes (1,8-ANS, Bis-ANS and Depoxyl sulfonic acid [Invitrogen, Oregon]) at three different concentrations (0.05 mM, 0.1 mM and 0.2 mM) to a total assay volume of 5 μL in a 384-well plate (Thermoscientific). To prevent evaporation, 1 μL of silicon oil (Sigma-Aldrich) was added to each well, and the plate was centrifuged at 1000 × *g* for 1 min. The Thermofluor experiment was performed in a ThermoFluor (Johnson & Johnson Pharmaceutical Research and Development, L.L.C) using the continuous ramping mode from 25°C to 8 °C in increments of 1°C, holding 1 min at each temperature. The results were analyzed using ThermoFluor++ software ver 1.3.7. 1,8-ANS dye gave the lowest background. The optimal protein and 1,8-ANS concentrations used for all subsequent assays were 0.4 mg/mL and 0.2 mM, respectively.

Fourteen compounds exhibiting dose-dependent titration from AlphaLISA and the HEK-Blue™ assay were screened against two constructs of ST2. Five microliters of buffer (10 mM HEPES 7.2, 150 mM NaCl) was added to each well in the 384-well plate, and then 50 nL of 50 mM stock compounds were added to the buffered wells with a pin tool. Reference wells contained 50 nL of DMSO without any compound. Five microliters of a 2x protein–dye solution was mixed in the wells and then overlaid with 2.5 μL of silicon oil. The final compound concentration in each well was 250 μM as the oil did not mix with the solutions. The plate was centrifuged at 1000 × *g* for 1 min. The Thermofluor experiment was performed using the same ramping mode described for the optimization, and the results were analyzed as detailed above. A compound causing a melting temperature shift of $\geq$0.5°C was considered an active binder and confirmed in quadruplicate measurements.

Liquid Chromatography-Mass Spectroscopy Analysis. Samples of ST2 with glycosylation from expression in Sf9 cells were analyzed using liquid chromatography followed by mass spectrometry (LC-MS). For LC-MS analysis, ST2 were purified in 25mM HEPES 7.5 and 150 mM NaCl then diluted to 1mg/ml with water. Each sample (0.5 uL) was separated by reverse phase HPLC (Phenomenex Aeris widepore C4 column 3.6 μM, 50 x 2.10 mm) at a flow rate of 0.5 mL/min in H_2O with 0.2% (v/v) formic acid. Protein was eluted using a gradient of 5-100% acetonitrile with 0.2% (v/v) formic acid over 4 minutes. Mass Spectra was collected on an Agilent Q-TOF 6545 carried out under the following conditions: fragment or voltage, 300 V; skimmer voltage, 75 V; nozzle voltage, 100 V; sheath gas temperature, 350 °C and drying gas temperature, 325 °C. MassHunter Qualitative Analysis Software (Agilent) was used for LC-MS data analysis. Intact protein masses were obtained using the maximum entropy deconvolution algorithm. The expected mass of ST2 (His-TEV-$ST2^{ECD}$**)** without glycolsylation is 37,138 Da.

MD Simulation. We modified our cosolvent MD simulation method (2) to detect the binding hotspot of iST2-1 in $ST2^{ECD}$. The rationale is that $ST2^{ECD}$ will be embedded with a higher concentration of iST2-1 as cosolvent molecules will undergo frequent interaction with iST2-1, thereby increasing the probability that iST2-1 will find its preferred binding

sites in $ST2^{ECD}$ in a shorter simulation time. A similar approach has been adopted in the study of drugs binding to Src kinase using a much diluted drug concentration and a longer simulation time (3). Binding hotspot mapping methods employing fragment-type molecules (Site Identification by Ligand Competitive Saturation) (4) or a mixed-solvent system (5) have also been reported previously. To prepare the equilibrated cosolvent solution of iST2-1, two stereospecific iST2-1 molecules and two chlorine ions were randomly placed in a box of 4096 water molecules in a ratio of iST2-1/water = 1/2800 using the Packmol program (6). Equilibration of the cosolvent solution was obtained by following previously reported protocols (2). To prepare the cosolvent MD simulation, the protonation state of ionizable groups in $ST2^{ECD}$ under the standard physiological condition was first assigned by the MOE program. After being capped with the N-methyl group (NME) and the acetyl group (ACE), $ST2^{ECD}$ was embedded in an octahedron box of the equilibrated cosolvent system in which the distance between any protein atom to the edge of the box was 13 Å. In the second simulation condition, the edge of the box to any protein atom was set at 15 Å. The total numbers of inhibitors in each simulation were 20 (S)-iST2-1 and 26 (R)-iST2-1 with the first box size and 29 (S)-iST2-1 and 31 (R)-iST2-1 with the latter (larger) box size. The total system was neutralized by adding counter ions (chlorine ions in this case) required by the periodic boundary condition involving charged species. The force field parameters used for $ST2^{ECD}$ and water molecules were the Amber 99SB force field parameters (7) and the TIP3P (8) model. For the glycosylated $ST2^{ECD}$, Amber 12SB force field parameters were used for the protein and GLYCAM-06j-1(9) force field parameters were used for three asparagine N-linked glycosylation in ST2. The force field parameters for stereo-specific iST2-1 were obtained using the Antechamber module in the Amber program suite following the same validated procedures from our previous studies (2, 10). All MD simulations were performed using the GPU modification to PMEMD (11) from Amber (version 14) (12). The protocols for preparation of the system and the production runs (32 ns) can be found in our previous study (13).

In the binding site detection (or cosolvent mapping (2)) analysis, an 8-ns window of cosolvent MD simulations was analyzed progressively from 0 to 32 ns to monitor the evolution and persistence of the preferred iST2-1 binding location on $ST2^{ECD}$. We have shown that the D1-D2 domain of apo-$ST2^{ECD}$ ($ST2^{ECD-D1D2}$) underwent limited conformational changes (1). Here, we aligned all snapshots of $ST2^{ECD}$ obtained from the cosolvent MD simulations to $ST2^{ECD-D1D2}$ taken from the crystal structure as a reference. The expected observation frequency of all heavy atoms of iST2-1 in the cosolvent system was set at an empirical value of 0.004320 for (S)-iST2-1 and (R)-iST2-1 to detect persistent residence of iST2-1 in $ST2^{ECD}$ for the entire 32 ns in the final analysis reported in Fig. 5. Because $ST2^{ECD-D1D2}$ accounts for 83% of the binding free energy between ST2 and IL-33 (1), we focused on identifying prolonged association of iST2-1 at the interface between $ST2^{ECD-D1D2}$ and IL-33 that will exert direct inhibition to ST2/IL-33 interaction.

Table S1. Parameters obtained from the SAXS analysis using SCÅTTER and PRIMUS.

Protein	R_g(Å)	V_c(Å^2)	MW(kDa)	D_{max}(Å)	χ^2 (S_{k2})	R_g(Å)[a]
Apo-ST2	31.38	404.7	42.4	85	2.99	29.49 ± 0.03
$ST2^{ECD}$/iST2-1	31.26	405.8	42.8	84	3.12	29.73 ± 0.07

[a] R_g calculated using PRIMUS (14).

Table S2. Human and mice antibodies used in this work.

I. Human			
Antibody	**Source**	**Clone**	**Fluorochrome**
CD45	eBioscience	2D1	PerCP-Cy5.5
CD3	eBioscience	OKT3	FITC
CD4	eBioscience	OKT4	PE/ PerCP-eFluor® 710
CD8	eBioscience	OKT8	FITC/APC
IFNγ	eBioscience	4S.B3	PE
IL-17	eBioscience	eBio64DEC17	APC
Foxp3	eBioscience	236A/E7	APC
II. Mouse			
Antibody	**Source**	**Clone**	**Fluorochrome**
CD4	eBioscience	GK1.5	PE/ PerCP-eFluor® 710
CD8α	eBioscience	53-6.7	FITC/ PE-CY7
CD8β	eBioscience	eBioH35-17.2 (H35-17.2)	PE
CD90	eBioscience	30-H12	FITC/ PE-CY7
Foxp3	eBioscience	FJK-16s	PE-CY7
T-bet	eBioscience	eBio4B10	PE
RORγt	eBioscience	B2D	APC
Gata3	eBioscience	TWAJ	eFluor® 660
IFNγ	eBioscience	XMG1.2	PE/ APC/ PerCP-Cy5.5
IL-17A	eBioscience	eBio17B7	PE/APC
IL-4	eBioscience	BVD6-24G2	PE-CY7

Table S3. Stability of ST2 inhibitors in mouse liver microsome in vitro.

Time (min)	iST2-2	iST2-1	iST2-4	Varapamil (Positive control)	iST2-3	Varapamil (Positive control)
$T_{1/2}$ (min)	0.79	0.73	4.39	3.18	4.9	3.04

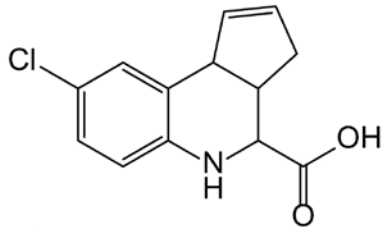

Chemdiv: CD1959-0211
AlphaLISA IC_{50} : 86.56 μM
HEK-Blue™ IC_{50} : no inhibition up to 75 μM
Thermal Shift :
ΔTm=1.47 °C at 200 μM, 0.77 °C at 200 μM*

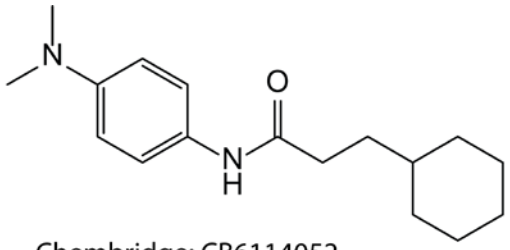

Chembridge: CB6114052
AlphaLISA IC_{50} : 70.2 μM
HEK-Blue™ IC_{50} : 34% inhibition at 75 μM
Thermal Shift :
ΔTm = 0.52 °C at 200 μM*

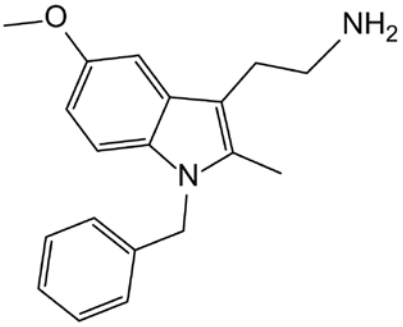

Chembridge: CB5107562
AlphaLISA IC_{50} : 70.7 μM
HEK-Blue™ IC_{50} : 33.55 μM
Thermal Shift :
ΔTm = 1.19 °C at 200 μM*

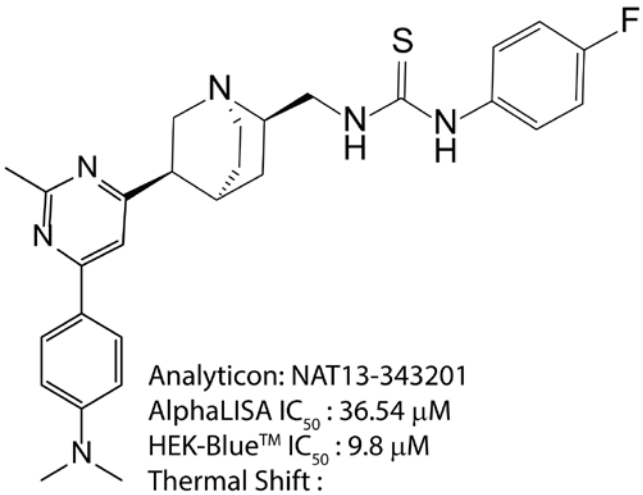

Analyticon: NAT13-343201
AlphaLISA IC_{50} : 36.54 μM
HEK-Blue™ IC_{50} : 9.8 μM
Thermal Shift :
ΔTm= 2.09 °C at 200 μM, 3.32 °C at 200 μM*

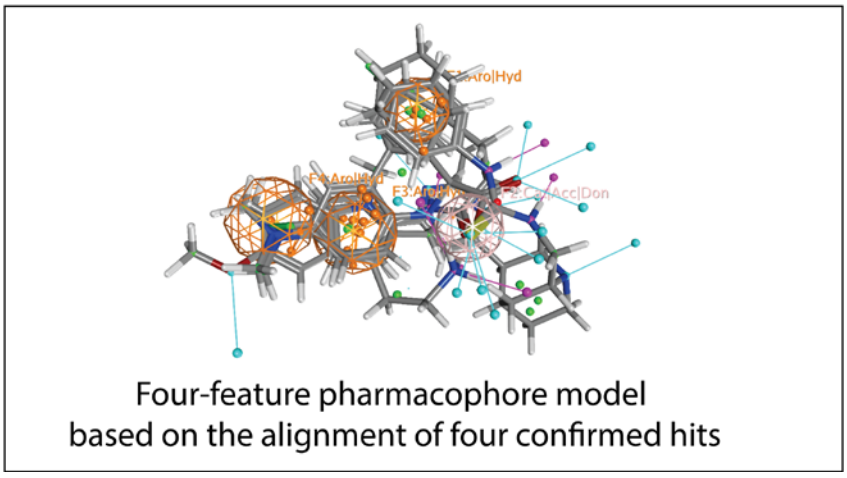

Figure S1. Four confirmed hits from primary screening and the alignment of their chemical structures in the pharmacophore model. The ΔTm observed in the thermal shift assay using the ST2(19-206) construct is marked with *.

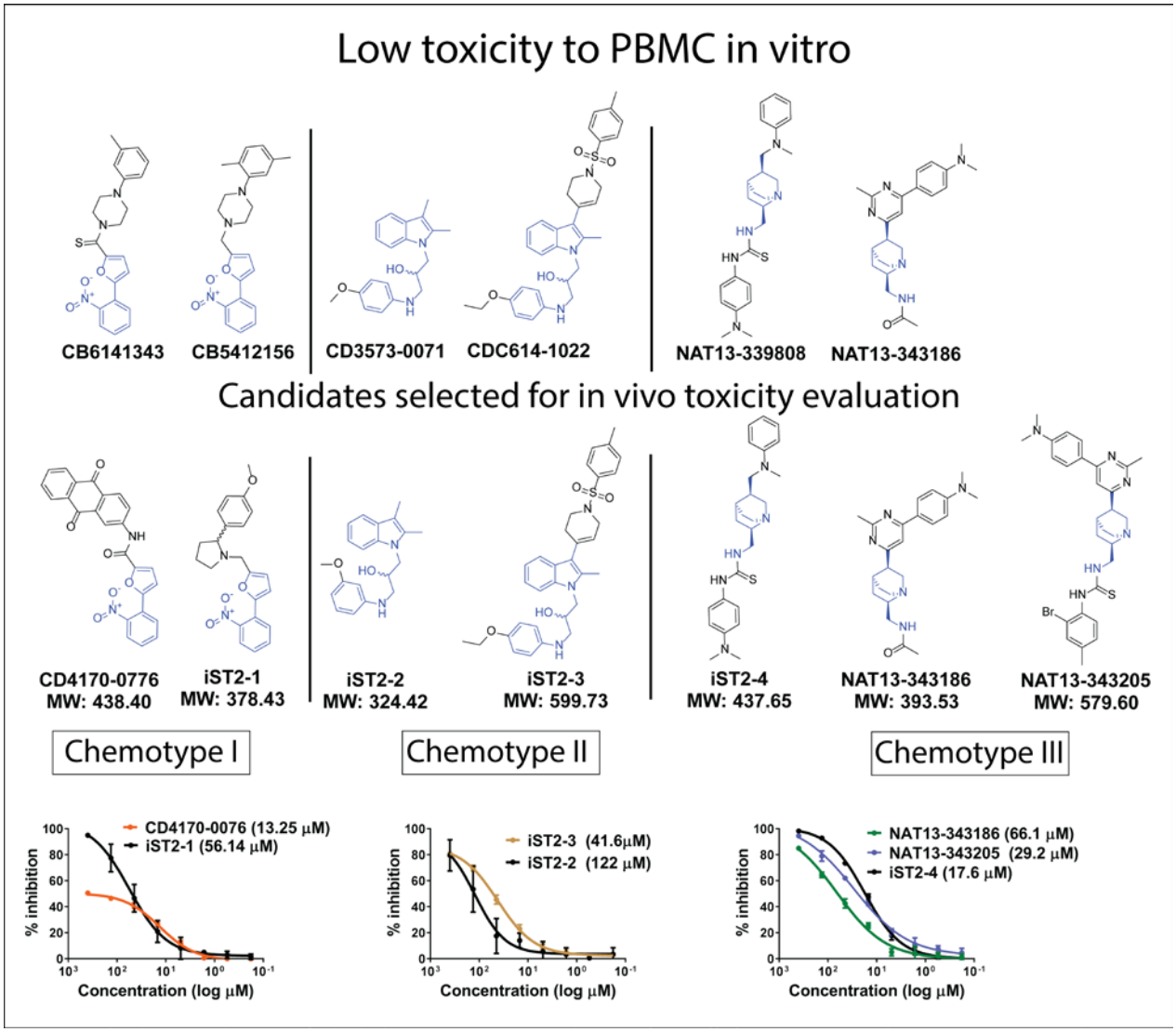

Figure S2. Chemical structures of selected candidate compounds yielding low toxicity in the in vitro and in vivo assays. Common scaffolds: (2-(2-nitrophenyl)furan for chemotype I, 1-(2,3-dimethyl-1H-indol-1-yl)-3-(phenylamino)propan-2-ol for chemotype II and quincoridine for chemotype III. The common scaffolds of each chemotype are colored in blue. CB, CD and NAT denote that the compounds were purchased from Chembridge, Chemdiv and Analyticon Discovery, respectively. Representative inhibition curves and the calculated IC_{50} values (in parentheses) determined from the AlphaLISA for the candidate compounds are provided. The data points and error bars correspond to >2 replicates.

A

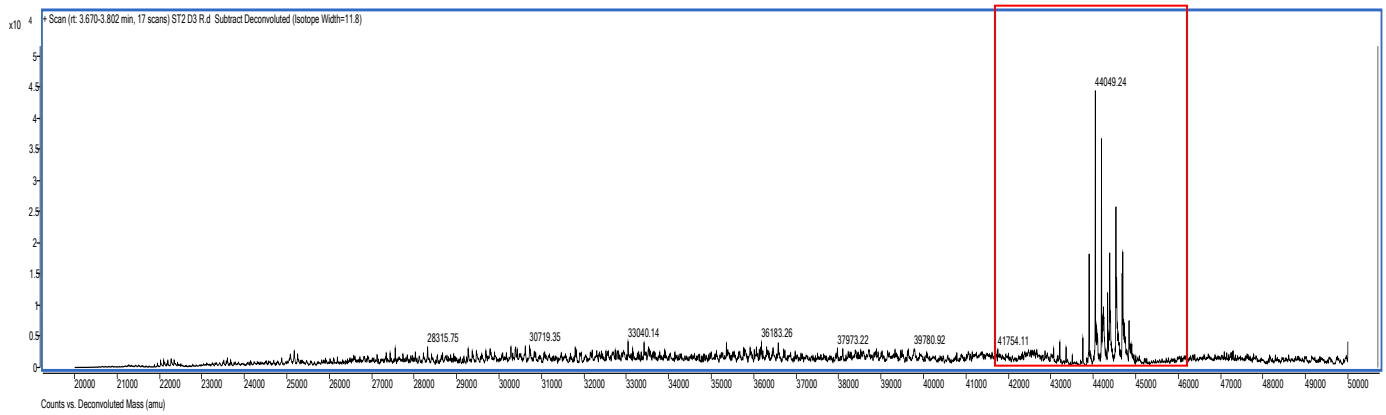

B

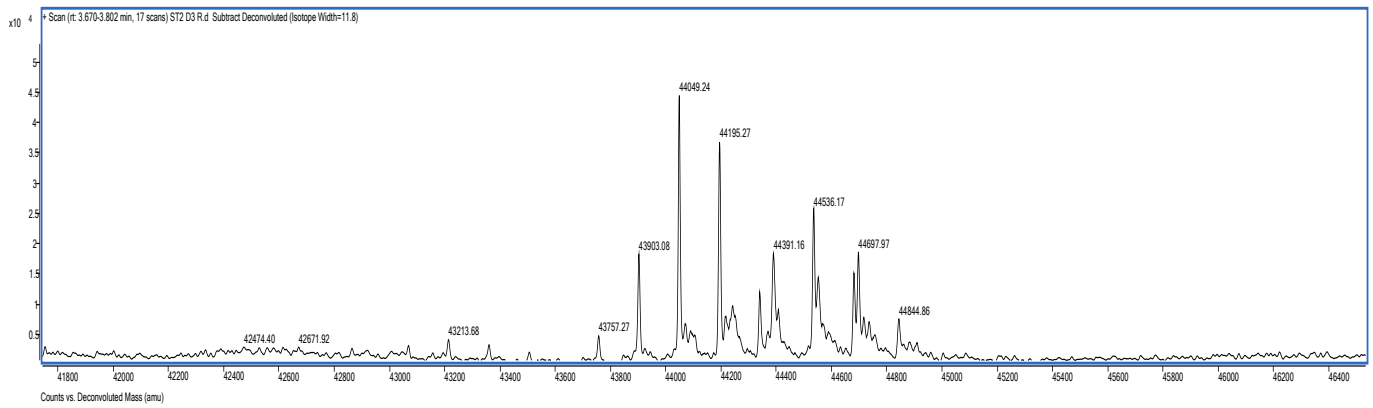

Figure S3. LC-MS analysis of ST2 (His-TEV-D1-3). (A) Mass spectra of ST2 (His-TEV-D1-3) glycosylated. (**B**) Inset of the red box region in (**A**).

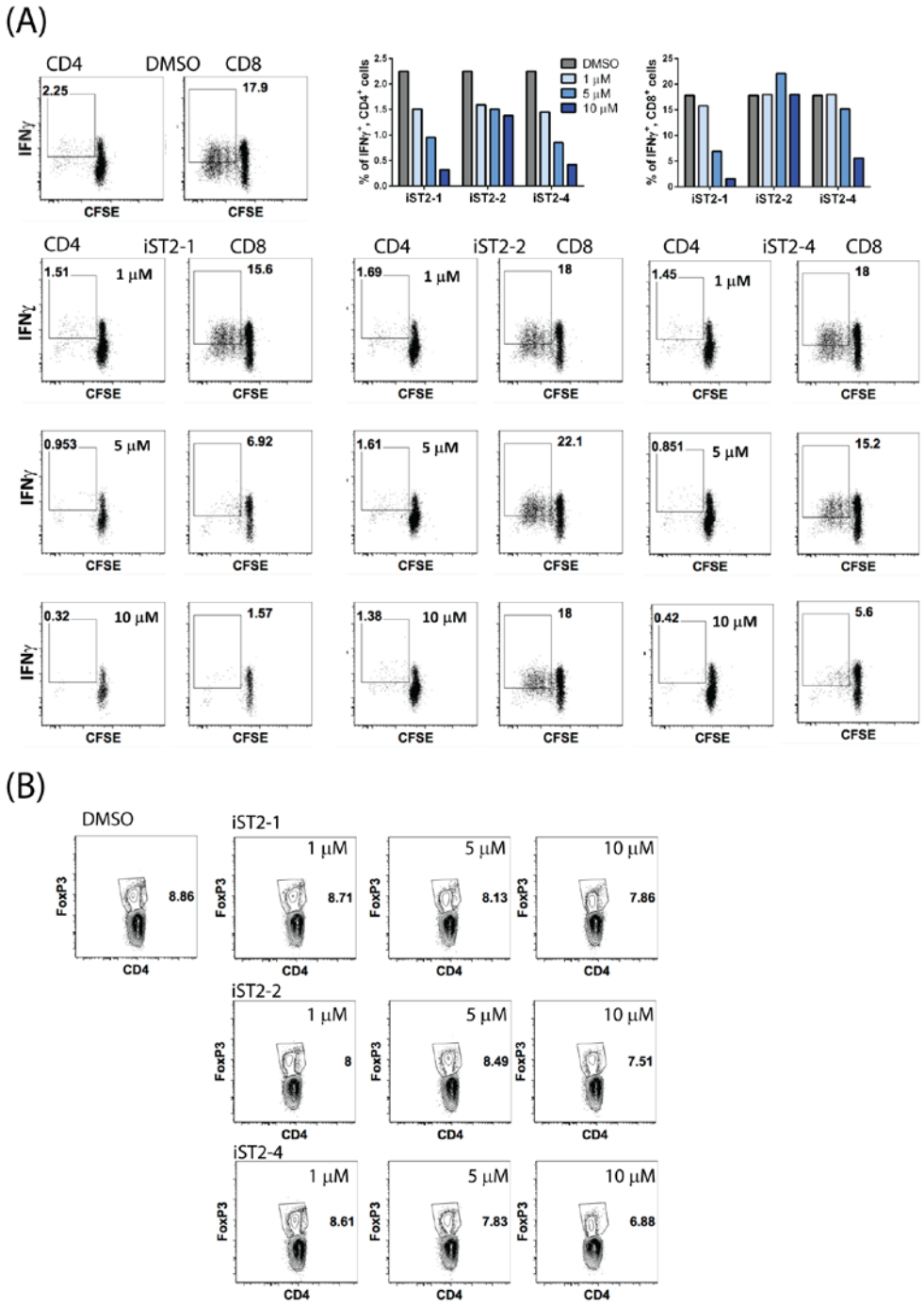

Figure S4. (A) IFNγ$^+$CD4$^+$ and IFNγ$^+$CD8$^+$ T-cell populations in the MLR incubated with ST2 inhibitors at 1–10 μM. Flow cytometric analysis of IFNγ$^+$CD4$^+$ and IFNγ$^+$CD8$^+$ cells among total T cells stained with CFSE in the MLR incubated with iST2-1, iST2-2, or iST2-4 at 1, 5 or 10 μM after 7 days. DMSO was used as the control. The ratio of responders (CD4$^+$ and CD8$^+$) to stimulators (irradiated T cell-depleted PBMCs) was 1:2. A summary of the T-cell populations is provided in the bar plot. **(B) FoxP3$^+$CD4$^+$ cell population in the MLR incubated with ST2 inhibitors at three concentrations.** Flow cytometric analysis of FoxP3$^+$CD4$^+$ cells among total T cells in the MLR incubated with iST2-1, iST2-2, or iST2-4 at 1, 5 or 10 μM after 7 days. DMSO was used as the control.

B6 -> C3H.SW (Day14)

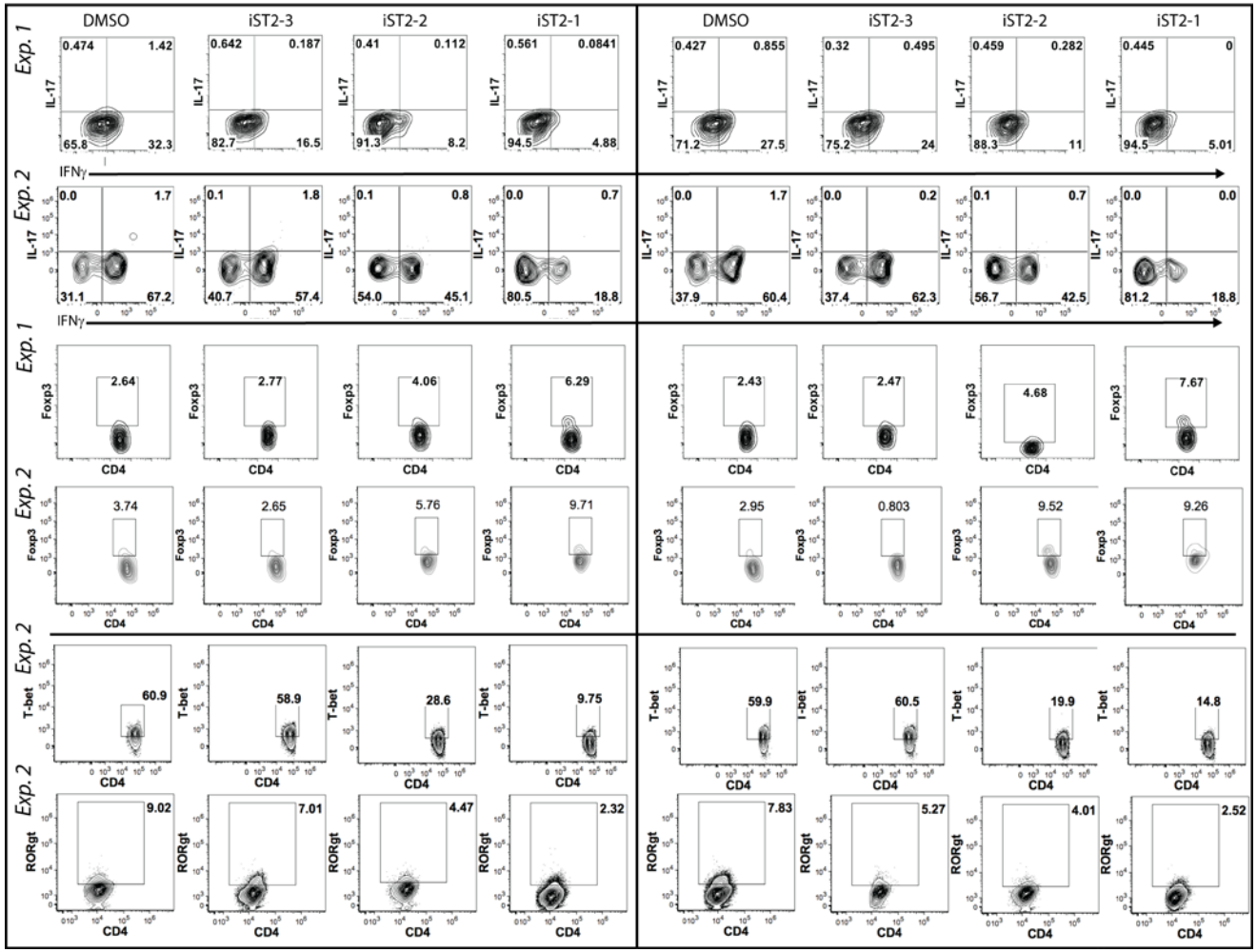

Figure S5. Ex vivo expression of IFN-γ and IL-17 (top) and Foxp3 (middle) T-bet and RORγt (bottom) in gut CD4 T cells collected on day 14 from the intestine of C3H.SW mice that received allogenic B6 T cells and bone marrow cells and were treated with ST2 inhibitors (n= 2 per group/experiment).

B6 -> C3H.SW (Day21) *Exp. 2*

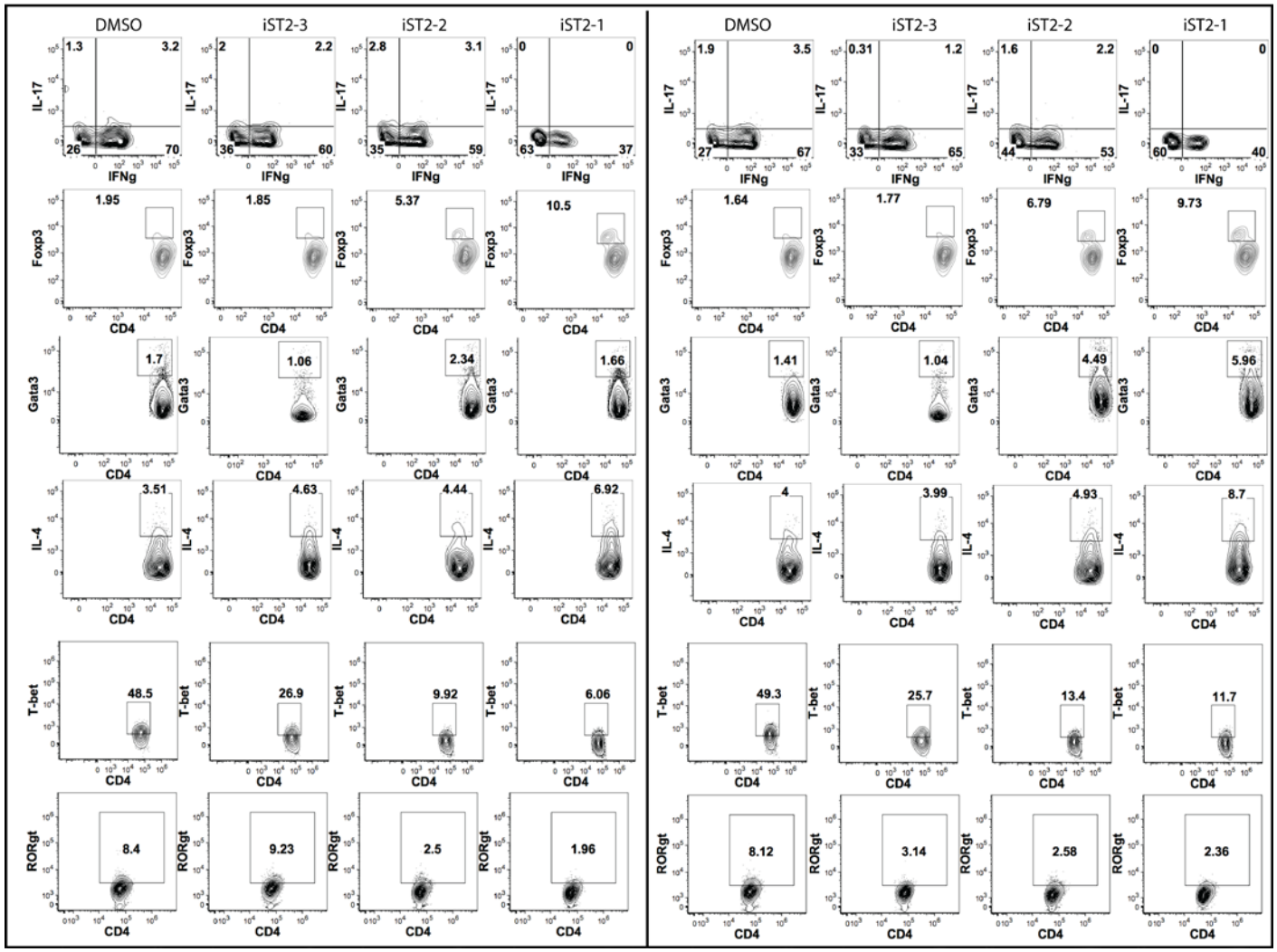

Figure S6. Ex vivo expression of IFN-γ, IL-17, Foxp3, Gata3, IL-4, T-bet and RORγt (in order) in gut CD4 T cells collected on day 21 from C3H.SW mice that received allogenic B6 T cells and bone marrow cells and were treated with ST2 inhibitors (n=2 per inhibitor).

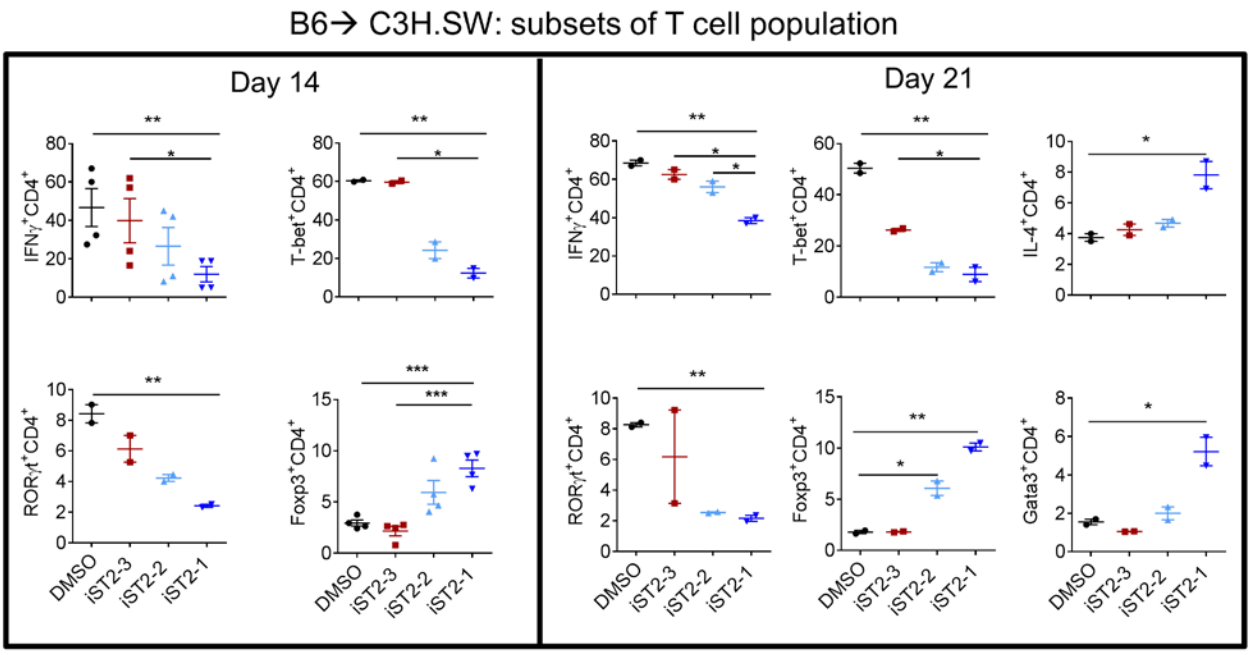

Figure S7. Summary of subsets of the T-cell population in the gut for the B6→C3H.SW model treated with ST2 inhibitors on days 14 (n=2) and 21 (n=2). Unpaired t-test, *p<0.05;p<0.01; ***p<0.001.**

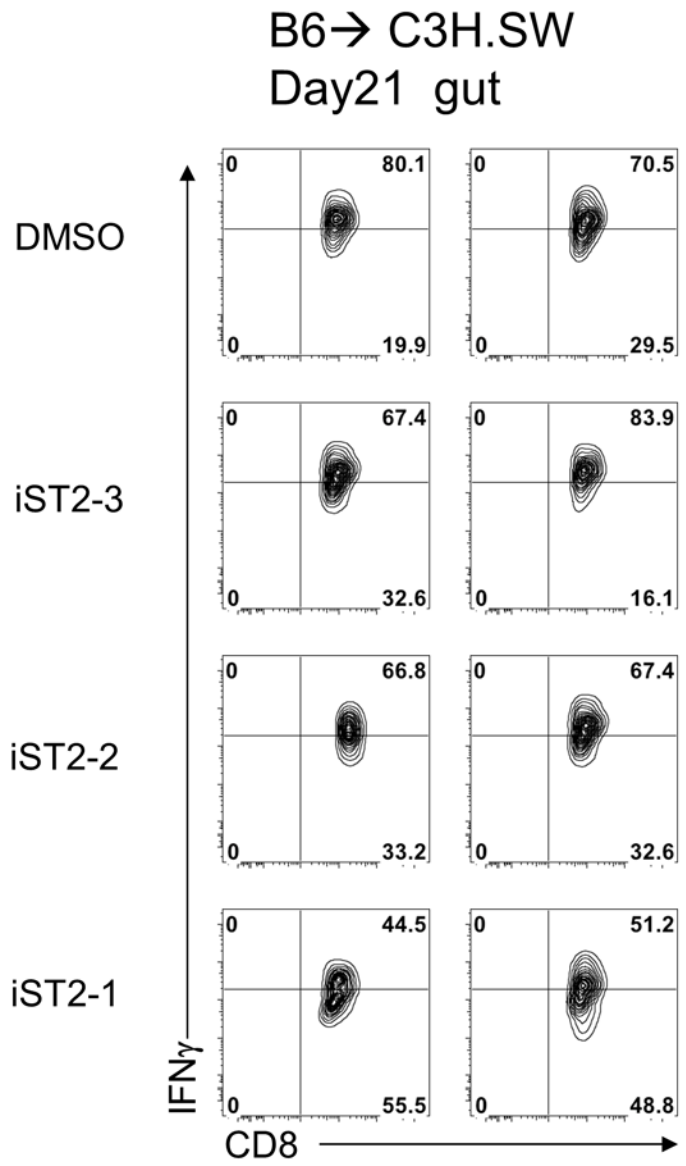

Figure S8. Ex vivo analysis of IFN-γ^+ CD8 T cells in gut collected on day 21 from the C3H.SW mice that received allogenic B6 T cells and bone marrow cells and were treated with ST2 inhibitors. (n=2 per inhibitor)

Reference

1. Yang CY, Delproposto J, Chinnaswamy K, Brown WC, Wang S, Stuckey JA, and Wang X. Conformational Sampling and Binding Site Assessment of Suppression of Tumorigenicity 2 Ectodomain. *PLoS ONE.* 2016;11(1):e0146522.
2. Yang C-Y, and Wang S. Analysis of Flexibility and Hotspots in Bcl-xL and Mcl-1 Proteins for the Design of Selective Small-Molecule Inhibitors. *ACS Medicinal Chemistry Letters.* 2012;3(4):308-12.
3. Shan Y, Kim ET, Eastwood MP, Dror RO, Seeliger MA, and Shaw DE. How does a drug molecule find its target binding site? *J Am Chem Soc.* 2011;133(24):9181-3.
4. Guvench O, and MacKerell AD, Jr. Computational fragment-based binding site identification by ligand competitive saturation. *PLoS Comput Biol.* 2009;5(7):e1000435.

5. Lexa KW, and Carlson HA. Full Protein Flexibility Is Essential for Proper Hot-Spot Mapping. *J Am Chem Soc.* 2011;133(2):200-2.
6. Martinez L, Andrade R, Birgin EG, and Martinez JM. PACKMOL: a package for building initial configurations for molecular dynamics simulations. *J Comput Chem.* 2009;30(13):2157-64.
7. Wang J, Cieplak P, and Peter A. Kollman. How well does a restrained electrostatic potential (RESP) model perform in calculating conformational energies of organic and biological molecules? *J Comput Chem.* 2000;21(12):1049-74.
8. Jorgensen WL, Chandrasekhar J, Madura JD, Impey RW, and Klein ML. Comparison of simple potential functions for simulating liquid water. *The Journal of Chemical Physics.* 1983;79(2):926-35.
9. Woods RJ, and Chappelle R. Restrained electrostatic potential atomic partial charges for condensed-phase simulations of carbohydrates. *Journal of Molecular Structure: THEOCHEM.* 2000;527(1):149-56.
10. Yang CY. Identification of potential small molecule allosteric modulator sites on IL-1R1 ectodomain using accelerated conformational sampling method. *PLoS ONE.* 2015;10(2):e0118671.
11. Salomon-Ferrer R, Götz AW, Poole D, Le Grand S, and Walker RC. Routine Microsecond Molecular Dynamics Simulations with AMBER on GPUs. 2. Explicit Solvent Particle Mesh Ewald. *Journal of Chemical Theory and Computation.* 2013;9(9):3878-88.
12. Case DA, Berryman JT, R.M.Betz, Cerutti DS, T.E. Cheatham I, Darden TA, E.Duke R, T.J.Giese, H.Gohlke, Goetz AW, et al. San Francisco: University of California; 2015.
13. Yang C-Y, and Wang S. Hydrophobic Binding Hot Spots of Bcl-xL Protein−Protein Interfaces by Cosolvent Molecular Dynamics Simulation. *ACS Medicinal Chemistry Letters.* 2011;2(4):280-4.
14. Konarev PV, Volkov VV, Sokolova AV, Koch MHJ, and Svergun DI. PRIMUS: a Windows PC-based system for small-angle scattering data analysis. *J Appl Crystallogr.* 2003;36(5):1277-82.